Efficient exciton energy transfer between widely separated quantum wells at low temperatures

A. Tomita* and J. Shah
AT&T Bell Laboratories, Holmdel, New Jersey 07733

R. S. Knox†
Laboratory for Laser Energetics, University of Rochester, Rochester, New York 14623-1299
(Received 7 September 1995)

Energy transfer between quantum wells is of fundamental interest and also contributes to the dynamical response of devices based on multiple quantum wells. We report the observation of efficient energy transfer at low temperatures between unequal GaAs quantum wells separated by a thick (10–30 nm) $Al_{0.3}Ga_{0.7}As$ barrier. The transfer efficiency is about 30% for transfer from the narrow well to the wide well (Stokes transfer), about 10^{-2}% for the anti-Stokes transfer, and nearly independent of temperature (2–80 K) and barrier thickness. Tunneling, thermal excitation, and impurity-related transitions cannot explain these observations. We present a calculation for transfer efficiency using Förster-type dipole-dipole interaction between excitons and between excitons and free carriers in quantum wells, and show that this dipole-dipole transfer process can reproduce the observed temperature dependence and the magnitudes of the transfer efficiency. This process has not been considered previously for energy transfer between quantum wells.

I. INTRODUCTION

Energy transfer between quantum wells separated by a barrier plays an important role in determining the dynamics of quantum well devices, such as quantum well laser diodes, quantum well optical modulators, and SEED's (self-electro-optic effect devices). The energy-transfer process is also of fundamental interest in semiconductor physics. Competition between the energy transfer and decay (of population or coherence) determines the optical response of the quantum wells. Therefore, one can obtain information on these processes from the optical response. Among the various energy-transfer processes, tunneling between wells and thermal excitation over the barriers have been expected to play a dominant role.

Tunneling of carriers[1,2] has been investigated in detail for both resonant and off-resonant conditions by various optical methods, such as time-resolved luminescence, four-wave mixing, pump-probe absorption, and photocurrent spectroscopy. These studies have shown that tunneling carries the excitation efficiently between quantum wells separated by a thin (typically less than 5 nm) barrier, but the energy-transfer time increases exponentially with barrier thickness.

Thermal activation over the barrier[3] is important at sufficiently high temperatures. At room temperature, for example, a fraction of carriers gains energy higher than the barrier by thermal excitation. These carriers can escape the potential well and contribute to the energy transfer. The energy-transfer rate (the inverse of energy transfer time) is expected to show activation-type dependence on temperature with activation energy of barrier height.

One might expect that the quantum wells separated by a thick barrier would be independent at low temperature, because the energy transfer is inefficient by tunneling and thermal excitation. In this paper, however, we will present quantum well luminescence results that show evidence of efficient energy transfer between wells separated by thick (10–30 nm) barrier at low temperature (2–80 K).[4] We propose that the dipole-dipole interaction between the wells, which does not need the overlapping of wave functions or thermal activation to escape the well, plays an important role in the energy transfer for such conditions. Energy transfer by the dipole-dipole interaction has been investigated extensively since first proposed by Förster,[5] and extended by Dexter.[6] The studies include phonon-assisted processes[7,8] in paramagnetic crystals (ruby, for example) and interaction between a sensitizer and band electrons.[9] These researchers have shown that this Förster-type energy transfer is quite effective for molecules in a solution, in crystals, and in thin-film multilayers. For quantum wells, however, it has not been considered except for energy transfer between the localized excitons at the islands in a single quantum well layer,[10] as a particular source of exciton linewidth,[11] and as the dominant exciton-exciton interaction mechanism in single quantum wells.[12,13] Recently, the influence of dipole-dipole coupling between quantum wells on the linear optical properties, for four-wave-mixing signals, and coherent and incoherent transport through the barrier has been investigated theoretically.[14]

II. EXPERIMENT

We have investigated three different $GaAs/Al_{0.3}Ga_{0.7}As$ quantum well samples, each consisting of a 10-nm-thick wide well (WW) and a 5-nm-thick narrow well (NW) separated by barriers of thickness $d=30$, 20, and 10 nm in samples *A*, *B*, and *C* respectively. Sample *A* has only one pair of WW and NW, whereas samples *B* and *C* contain ten pairs separated by 50-nm barriers. These wells and barriers are nominally undoped. We have measured cw photoluminescence (PL) and photoluminescence excitation (PLE) at various excitation and detection energies as a function of temperature and excitation density. The samples were excited by a tunable cw Ti-doped sapphire laser. The luminescence was analyzed by a monochromator and detected by photon counting.

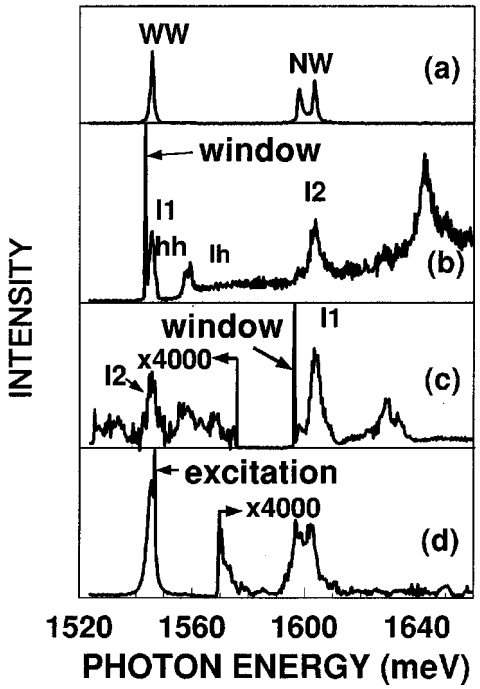

FIG. 1. (a) Photoluminescence (PL) spectrum of sample A ($d=30$ nm) at 40 K excited at 1720 meV. WW denotes luminescence from wide-well excitons, whereas NW denotes luminescence from narrow-well excitons. (b) Photoluminescence excitation (PLE) spectrum for luminescence from the wide-well excitons. The line ''window'' shows the position of the monochromator spectral window. I_1 denotes the intensity of the WW PL for excitation at the WW, and I_2 denotes the intensity of the WW PL for excitation at the NW exciton. The peak at 1640 meV is due to the e_2-hh_2 transition in the WW. (c) PLE spectrum for the NW exciton luminescence. I_1 and I_2 denote intensity of the NW PL for excitation at the NW and WW, respectively. (d) PL spectrum excited at the wide-well exciton energy. Luminescence from the narrow-well excitons was induced by this excitation.

Figure 1(a) shows the PL spectrum excited at 1720 meV, i.e., higher than the lowest interband transition energies in both the WW and NW quantum wells. Two peaks corresponding to WW and NW excitons were observed (the NW luminescence was split because of well width fluctuation). The energy separation between the NW and WW excitons is about 60 meV. Figure 1(b) shows the PLE spectrum of the WW heavy-hole exciton in sample A at 40 K. The WW luminescence is clearly enhanced by the excitation of the NW exciton energy (peak labeled $I2$). The $I2$ peak persists when the window of detection is changed to the center of the WW exciton. These observations provide convincing evidence for energy transfer from NW to WW (Stokes-type transfer). This enhancement was observed even at 2 K for all three samples. We define here three quantities: $I1$, the WW exciton luminescence intensity by direct excitation (excitation at the WW energy), $I2$, the WW exciton luminescence intensity by energy transfer from the NW (excitation at the NW exciton), and the ratio $I2/I1$. We will refer to this ratio as the transfer efficiency for the Stokes-type transfer. The contribution from the continuum states of the WW must be subtracted to obtain $I2$. The transfer efficiency is closely related to the transfer time τ_{tr}:

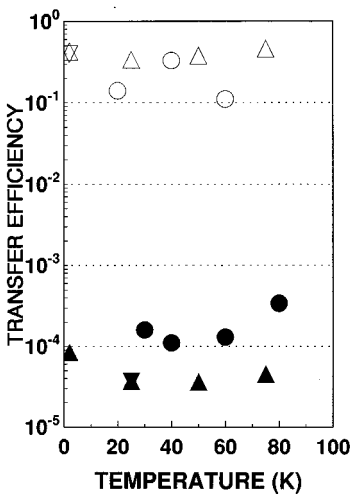

FIG. 2. Summary of transfer efficiency for exciton energy transfer. Open symbols, Stokes transfer; filled symbols, anti-Stokes transfer. Sample A ($d=30$ nm): circles; Sample B ($d=20$ nm): triangles; Sample C ($d=10$ nm): inverted triangles.

$$\frac{I2}{I1}=\frac{1}{1+\tau_{\mathrm{tr}}/\tau_2}\,\frac{\alpha_2 L_2}{\alpha_1 L_1}, \tag{1}$$

where τ_2 is the NW exciton lifetime, α_1 and α_2 are the absorption coefficients, and L_1 and L_2 are the well thicknesses for the WW (subscript 1) and NW (subscript 2). Observed values for the transfer efficiency are $\approx$30%, which shows fairly strong energy transfer from NW to WW. Using the values of α_2/α_1 measured by Masumoto *et al.*,[15] we obtain values for $\tau_{\mathrm{tr}}/\tau_2$ of approximately 10. The transfer efficiency is nearly independent of temperature and does not show any apparent dependence on the barrier thickness, as summarized in Fig. 2.

Figures 1(c) and 1(d) show the energy transfer from WW to NW (anti-Stokes type transfer) in sample A at 40 K. The PLE spectrum for the NW luminescence is shown in Fig. 1(c) and the PL spectrum excited at the WW exciton energy is depicted in Fig. 1(d). As seen in the figures, the luminescence at the NW exciton energy was also enhanced by the excitation at the WW energy. The luminescence spectrum at the NW exciton energy reproduces the doublet structure seen in Fig. 1(a), which indicates that the observed luminescence is due to NW exciton recombination. The enhancement was observed for all the samples at 2–80 K. When the temperature was higher than 80 K, the tail of the WW luminescence covered the NW luminescence, as seen in Fig. 3. The exciton temperature estimated from the WW luminescence tail was less than 5 K higher than the lattice temperature. We define the transfer efficiency by the ratio $I2/I1$. This time, the direct excitation luminescence intensity $I1$ is the excitation peak at the NW exciton energy and the energy-transfer-related luminescence intensity $I2$ is the excitation peak at the WW exciton in the PLE spectrum. We can use the relation, Eq. (1), by redefining the indices as $1\rightarrow N$ and $2\rightarrow W$. We can estimate the transfer time from the PL spectrum, but we need the ratio of the quantum efficiency between WW and NW. This ratio depends on sample quality and may bring about uncertainty in the result for transfer times. Therefore, we use the transfer efficiency values obtained from the PLE

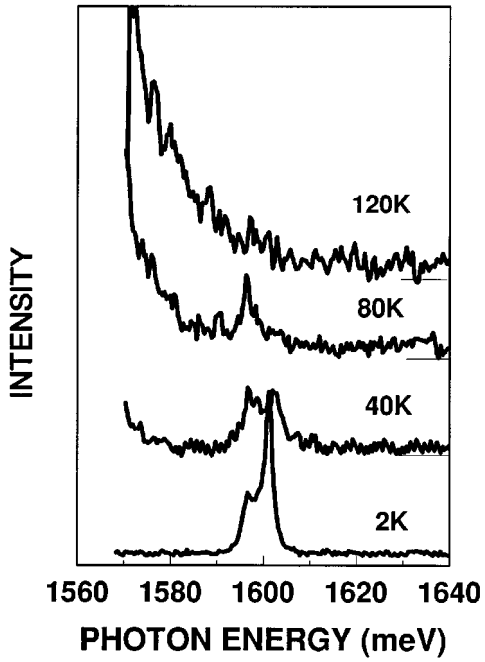

FIG. 3. Temperature dependence of the photoluminescence line shape for sample *A* excited at the wide-well exciton energy.

for further analysis. Figure 2 shows a summary of transfer efficiency values. The anti-Stokes energy-transfer efficiency was 10^{-3} times that of the Stokes transfer. The efficiency was again nearly independent of temperature. The values are more scattered from sample to sample than for Stokes transfer.

In order to estimate the transfer probability $1/\tau_{tr}$ from Eq. (1), we have measured the lifetimes of the WW and NW excitons in all samples, as a function of temperature by time-resolved luminescence.[16] Figure 4 shows the measured exciton lifetimes. The lifetime values in a single quantum well (sample *A*) are $\frac{1}{10}$ to $\frac{1}{2}$ of those in multiple quantum wells (samples *B* and *C*). The lifetime for the WW excitons decrease as the temperature increases, whereas the lifetime for the NW excitons increases. The temperature dependence of the lifetime is smaller in sample *A* than in samples *B* and *C*.

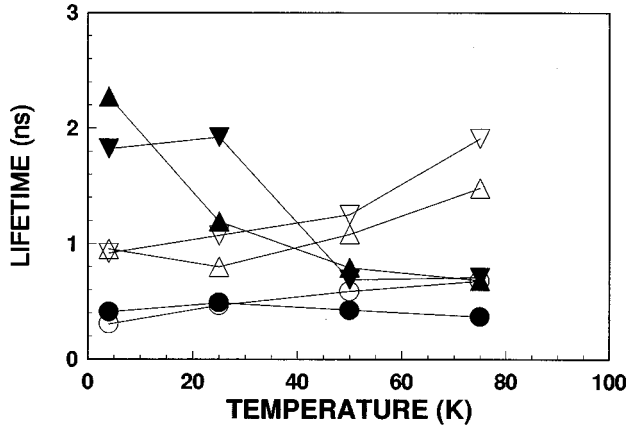

FIG. 4. Exciton lifetime as a function of temperature. Open symbols, wide-well excitons; filled symbols, narrow-well excitons. Sample *A* (d=30 nm): circles; Sample *B* (d=20 nm): triangles; Sample *C* (d=10 nm): inverted triangles.

Using these lifetimes and the measured transfer efficiencies, we determine the transfer probabilities for the Stokes and anti-Stokes transfer at various temperatures. These values are shown for all three samples as different symbols in Figs. 5(a) and 5(b) for the anti-Stokes and Stokes transfers, respectively. The solid curves are calculated using the dipole-dipole interaction theory developed in the next section.

III. THEORY

A. Förster-mechanism transfer rate

We first consider the dipole-dipole interaction as an energy-transfer mechanism. In this section, we will concentrate on the direct exciton-to-exciton energy transfer. Phonon-assisted transfer can be ruled out, because its temperature dependence should show activation-type behavior resulting from thermal distribution of the phonons for anti-Stokes-type transfer. Moreover, the phonon-assisted interaction should be weak, because one-phonon processes cannot contribute to anti-Stokes energy transfer under the present experimental conditions; the energy separation (~60 meV) is larger than the LO phonon energy (37 meV) and the largest acoustic-phonon energy.

Excitons can transfer to free-electron-hole states by dipole-dipole interaction. This should be important for Stokes transfer, because it satisfies energy conservation directly. The free electron-hole pairs rapidly (in tens of ps) relax to excitons before recombination and contribute to the WW exciton luminescence. For anti-Stokes transfer, however, this interaction should be negligible, because there is no energy-conserving counterpart in the NW and the matrix element is smaller than that of exciton-to-exciton transfer. We can neglect transfer from free-electron-hole pairs to excitons, because the free-carrier population is much smaller than that of excitons, because of resonant excitation of excitons in the WW and low temperatures.

One might think that direct exciton-to-exciton transfer would be extremely weak, because of the wide energy separation (~60 meV) between the WW and NW quantum levels. Nevertheless, we show below that the finite exciton linewidth yields a finite value for the overlap integral of the WW excitons and the NW excitons. This overlap integral is essential to energy transfer via the Förster-Dexter process[5,6] and must be regarded in our context as an accounting for multiphonon processes.

We derive here the transition rate for the direct exciton-to-exciton energy transfer important for anti-Stokes transfer. That for energy transfer from the exciton to free-electron-hole pair states is derived in B. First, we define the initial and final states for exciton energy transfer in quantum wells as[17]

$$|i\rangle=|mn\nu\mathbf{K}\rangle=\Big[N^{-1/2}\sum_{R}e^{i\mathbf{K}\cdot\mathbf{R}}\sum_{\boldsymbol{\beta}}F_{\nu}(\boldsymbol{\beta})\times\Psi_{mn}(\mathbf{R},\mathbf{R}+\boldsymbol{\beta})\Big]\Psi_{g2},$$
$$|f\rangle=|m'n'\nu'\mathbf{K}'\rangle=\Psi_{g1}\Big[N^{-1/2}\sum_{\mathbf{R}'}e^{i\mathbf{K}'\cdot\mathbf{R}'}\sum_{\boldsymbol{\beta}'}F_{\nu'}(\boldsymbol{\beta}')\times\Psi_{m'n'}(\mathbf{R}',\mathbf{R}'+\boldsymbol{\beta}')\Big], \quad (2)$$

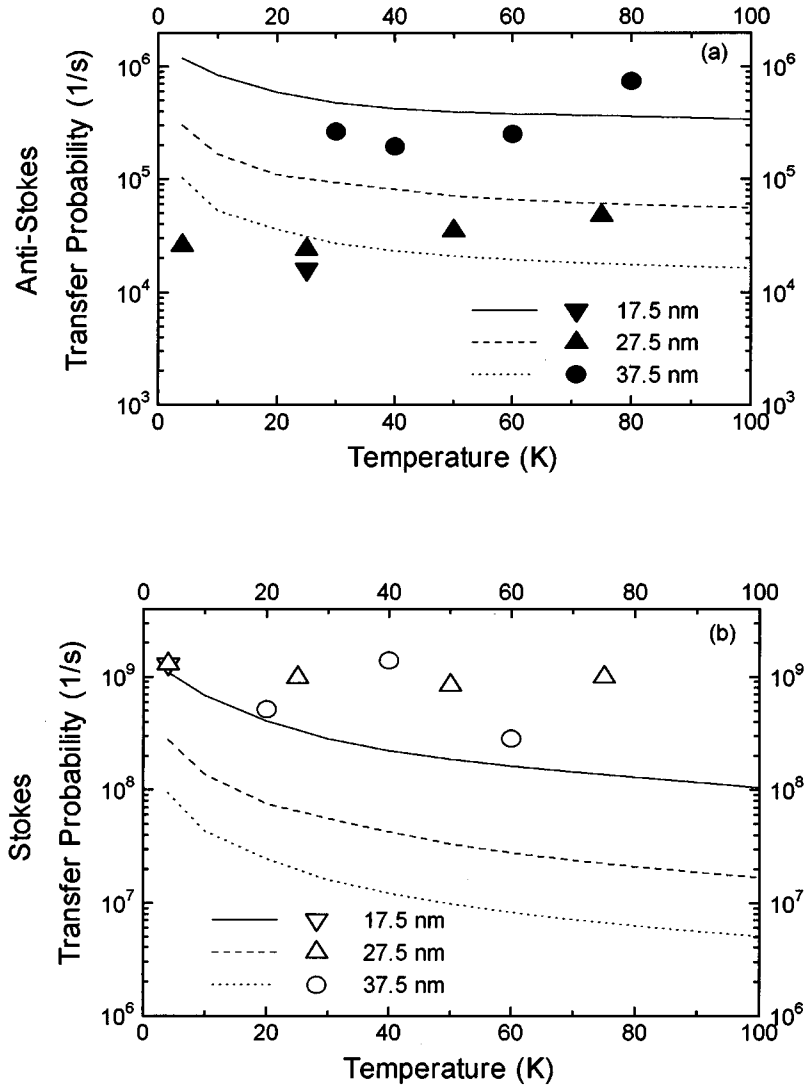

FIG. 5. Calculated temperature dependence of the transfer probability for *anti-Stokes* transfer (upper figure) and for Stokes transfer (lower figure) using a value of 5.5 e Å for the dipole moment. Lines represent the calculations and symbols represent the experimental results. Parameter b represents the distance between the center planes of the two quantum wells and equals the barrier thickness (d) plus one-half of the sum of the well thicknesses. Sample A: $b=37.5$ nm; Sample B: $b=27.5$ nm; and Sample C: $b=17.5$ nm.

where the states in the square brackets are linear combinations of the one-electron excited states in which an m (m') valence-band electron in the $\mathbf{R}$ ($\mathbf{R}'$) cell has been removed to an n (n') conduction band in the $\mathbf{R}+\boldsymbol{\beta}$ ($\mathbf{R}'+\boldsymbol{\beta}'$) cell with center-of-mass momentum $\mathbf{K}$ ($\mathbf{K}'$). The primes indicate well 2, in which the final state resides, and no primes indicate well 1, in which the initial state resides. Functions Ψ_{1g} and Ψ_{2g} denote ground states for wells 1 and 2, respectively. The envelope functions $F_\nu(\boldsymbol{\beta})$ and $F_{\nu'}(\boldsymbol{\beta}')$ ensure that the linear combinations are Wannier exciton states, i.e., that the Hamiltonian is diagonal for the individual wells. Motion in the z direction (perpendicular to the well layer) within the wells is ignored in this analysis. The energies of the initial and final states are assumed to be $E_i(\mathbf{K})=E_1+(\hbar^2K^2/2M)$ and $E_f(\mathbf{K}')=E_2+(\hbar^2K'^2/2M)$.

The Coulomb interaction V conserves the total momentum $\mathbf{K}$ in the x-y plane. The lattice sums over $\mathbf{R}$ and $\mathbf{R}'$ are, therefore, taken over R_x and R_y, which are aligned with R_x' and R_y'. The interwell coupling induced by V,

$$\langle f|V|i\rangle = N^{-1}\sum_{\substack{\mathbf{R},\mathbf{R}'\\(x,y)}} e^{-i(\mathbf{K}\cdot\mathbf{R}-\mathbf{K}'\cdot\mathbf{R}')}\sum_{\boldsymbol{\beta}}\sum_{\boldsymbol{\beta}'} F_\nu(\boldsymbol{\beta})^* F_{\nu'}(\boldsymbol{\beta}') \times\langle\Psi_{mn}(\mathbf{R},\mathbf{R}+\boldsymbol{\beta})\Psi_{2g}|V|\Psi_{1g}\Psi_{m'n'}(\mathbf{R}',\mathbf{R}'+\boldsymbol{\beta}')\rangle, \quad (3)$$

simplifies to

$$\langle f|V|i\rangle = \delta_{\mathbf{K},\mathbf{K}'}\sum_{\mathbf{R}} e^{i\mathbf{K}\cdot\mathbf{R}}F_\nu(0)F_{\nu'}(0) \times\langle\Psi_{mn}(0,0)\Psi_{2g}|V|\Psi_{1g}\Psi_{m'n'}(\mathbf{R},\mathbf{R})\rangle, \quad (4)$$

if we assume that only the $\boldsymbol{\beta}$ and $\boldsymbol{\beta}'=0$ terms can contribute to the transition moments, which is appropriate for allowed transitions. The bracket on the right-hand side of Eq. (4) is the coupling matrix element between states in which excitation is localized at the origin of the left well and at $\mathbf{R}$ in the

right well. The transfer probability w_{fi} will be calculated by adapting the well-known Förster-Dexter formalism[5,6] as follows:

$$w_{fi}=\left\langle \frac{2\pi}{\hbar}\sum_f \left|\langle f|V|i\rangle\right|^2 \rho_f^{\rm eff}(E_f,E_i)\right\rangle_i , \tag{5}$$

where $\rho_f^{\rm eff}(E_f,E_i)$ is an effective density of final states. The bracket $\langle\ \rangle_i$ stands for a thermal average over initial states. In the usual context of time-dependent perturbation theory, the letters ''*i*'' and ''*f*'' on the left refer to manifolds of similar initial and final states between which the transition is occurring. We will relate the effective density of states to spectral overlapping using Förster's method, which involves extracting optical strengths from the transition matrix element and combining them with a normalized donor-well emission spectrum and a normalized acceptor-well absorption spectrum.

In our application of Eq. (5), the average over initial states is simplified by the circumstance that the matrix element, Eq. (4), depends only on K, the magnitude of $\mathbf{K}$. This is demonstrated in Appendix A, where it is shown that the effective value of $|\langle f|V|i\rangle|^2$ is

$$\begin{aligned}|\langle f|V|i\rangle|^2 &= \delta_{\mathbf{K},\mathbf{K}'}2\left|F_\nu(0)F_{\nu'}(0)\sum_{\mathbf{R}} e^{i\mathbf{K}\cdot\mathbf{R}}\left[\frac{\mu_f\cdot\mu_i-3(\mu_f\cdot\mathbf{R})(\mu_i\cdot\mathbf{R})}{\varepsilon R^3}\right]\right| \\ &= \delta_{\mathbf{K},\mathbf{K}'}2|F_\nu(0)F_{\nu'}(0)|^2\left(\frac{2\pi n_a\mu_f\mu_i}{\varepsilon b}\right)^2\left(2-Kb+\frac{K^2b^2}{4}\right)\exp(-2Kb) \\ &= \delta_{\mathbf{K},\mathbf{K}'}2\left(\frac{16\mu_f\mu_i}{a_B^2\varepsilon b}\right)^2\left(2-Kb+\frac{K^2b^2}{4}\right)\exp(-2Kb),\end{aligned} \tag{6}$$

where n_a is the (two-dimensional) density of acceptor sites, μ_f and μ_i are transition dipole moments evaluating between valence- and conduction-band Wannier states within the same cell in the acceptor and donor wells, respectively, ε is the average optical dielectric constant of the medium between and within wells, b is the center-to-center distance between the wells, and a_B is the bulk exciton Bohr radius. The principal assumptions made in obtaining (6) are that the transition moments are in the plane of the wells, that there are degenerate exciton states having these moments along both the x and y directions, that the effect of well thickness on the xy motion is negligible, and that the degeneracy of the excitons is lifted entirely by the quantum effect in the z direction.

Because the quantity that we wish to average is a function only of the magnitude of $\mathbf{K}$, the average over initial states may be performed without difficulty. The general form of such an average is

$$\begin{aligned}\langle f(K)\rangle_i &= \frac{\sum_{\mathbf{K}} g_{mn\nu}(\mathbf{K})\exp[-E_{mn\nu}(K)/k_BT]f(K)}{\sum_{\mathbf{K}} g_{mn\nu}(\mathbf{K})\exp[-E_{mn\nu}(K)/k_BT]} \\ &= \frac{\int_0^\infty kK\ dK\ \exp[-E(K)/k_BT]f(K)}{Mk_BT/\hbar^2},\end{aligned} \tag{7}$$

in which we have used the K-independent density of states for a particle of mass M: $g_{mn\nu}(\mathbf{K})\approx MA/\pi\hbar^2$, where A is the normalization area. In (7) the factor A/π cancels out between the numerator and denominator, whereas the factor $M/\hbar^2$ does not, because the integral in the denominator has been transformed into an integral over energy.

Before performing the thermal average, we must still consider the density of final states and the sum over the final states. Anticipating use of the Förster method, we approximate the final-state density by a Lorentzian $\rho^{\rm eff}(E_f,E_i)\approx\Delta(E_f-E_i)$, the width of which will be discussed in Sec. C 3. Since the Förster method relates the dipole-allowed transitions in the transfer process to those of optical transitions, the width of the Lorentzian will derive from the overlap integral between the donor emission and the acceptor absorption states. As to the sum over the final states, the momentum-conservation δ function in the electronic interaction $\delta_{\mathbf{K},\mathbf{K}'}$ simplifies the calculation, because the Lorentzian $\Delta(E_f-E_i)=\Delta[E_2+(\hbar^2K'^2/2M)-E_1-(\hbar^2K^2/2M)]$ may be replaced by $\Delta(E_2-E_1)$. It is noteworthy that a sum is not made over the layers of the quantum well, as it would be in the case of a molecular multilayer with tightly bound excitons. The strong coupling within the well raises the degeneracy associated with the z motion, reducing the well effectively to a monolayer.

We are now prepared to evaluate the transition probability (5) by substituting the following expression into (7):

$$\begin{aligned}f(K) &= \frac{2\pi}{\hbar}|\langle f|V|i\rangle|^2\rho_f^{\rm eff}(E_f,E_i) \\ &= \frac{4\pi}{\hbar}|\langle f|V|i\rangle|^2\Delta(E_2-E_1) \\ &= \frac{4\pi}{\hbar}\left(\frac{16\mu_f\mu_i}{a_B^2\varepsilon b}\right)^2\left(2-Kb+\frac{K^2b^2}{4}\right)\exp(-2Kb) \\ &\quad\times\Delta(E_2-E_1).\end{aligned} \tag{8}$$

The thermal average affects only the K-dependent factors, and it is convenient to introduce the dimensionless function,

$$a(u)=\left\langle\left(2-Kb+\frac{K^2b^2}{4}\right)\exp(-2Kb)\right\rangle_i, \tag{9}$$

which is expressible in terms of the complementary error function:

$$a(u)=\tfrac{1}{4}[u^4+5u^2+8-(2u^4+11u^2+20) \times(\sqrt{\pi}/2)u\ \exp(u^2)\mathrm{erfc}(u)], \tag{10}$$

where $u=b/\lambda_T$ and $\lambda_T=\sqrt{\hbar^2/2Mk_BT}$ is the thermal wavelength. The function *a(u)* has interesting limiting properties and is discussed in Appendix B. For present purposes, it is sufficient to know that it has an asymptotic form

$$a(u)=\frac{11}{16u^2}\left(1-\frac{15}{11u^2}+\cdots\right), \tag{11}$$

which is reliable to within 1% for $u>8$ when only two terms in the series are used. Over the useful intermediate range of $u=4$ through 14, its value is given to similar accuracy by the interpolation formula $a(u)=0.5887u^{-1.937}$. Numerical methods are necessary for accurate evaluation when $u<4$. To emphasize the physical parameters on which $a(u)$ depends, we will write $a(b,T)$.

The transition probability now takes the form

$$w_{fi}^{\text{anti-Stokes}}=\frac{4\pi}{\hbar}\left(\frac{16\mu_f\mu_i}{a_B^2\varepsilon b}\right)^2 a(b,T)\Delta(E_2-E_1). \tag{12}$$

The temperature dependence is contained in the last two factors. Since $a(b,T)$ is essentially proportional to b^{-2}, the overall spacing dependence of the rate is b^{-4}, as expected in the case of an inverse-sixth power summed over a sheet.

B. The Stokes case

Before numerical application, we modify the theory for the Stokes case. The mechanism is the same, a dipole-dipole resonance, so that most of the formalism carries over. The principal change is that the final state is now the free-electron pair state,

$$|f\rangle=|m'n'\mathbf{k}'\mathbf{K}'\rangle = \Psi_{g1}\left[N^{-1}\sum_{\mathbf{R}'}\ \sum_{\boldsymbol{\beta}'}\ e^{i(\mathbf{K}'\cdot\mathbf{R}'-\mathbf{k}'\cdot\boldsymbol{\beta}')}\Psi_{m'n'}(\mathbf{R}',\mathbf{R}'+\boldsymbol{\beta}')\right], \tag{2'}$$

replacing the final state in Eq. (2). If we apply the previous assumption that only the $\boldsymbol{\beta}=\boldsymbol{\beta}'=0$ terms contribute to the transition moments, this yields the matrix element

$$\langle f|V|i\rangle=\delta_{\mathbf{K},\mathbf{K}'}\sum_{\substack{\mathbf{R},\mathbf{R}'\\(x,y)}} e^{i\mathbf{K}\cdot\mathbf{R}}F_\nu(0)* \times\langle\Psi_{mn}(0,0)\Psi_{2g}|V|\Psi_{1g}\Psi_{m'n'}(0,0)\rangle. \tag{3'}$$

Thus, compared with the earlier calculation, one exciton envelope function $F_{\nu'}(0)$ disappears. The function (8), that is to be thermally averaged becomes

$$f(K)=\frac{2\pi}{\hbar}\sum_{\mathbf{k},',\mathbf{K}'}|\langle f|V|i\rangle|^2\rho_f^{\text{eff}}(E_f,E_i) =\frac{2\pi}{\hbar}\frac{1}{N}\sum_{\mathbf{k}'\mathbf{K}'}|F_\nu(0)|^2|D_{fi}|^2\delta_{\mathbf{K},\mathbf{K}'}\delta(E_f-E_i) =\frac{2\pi}{\hbar}|F_\nu(0)|^2\frac{md^2}{\pi\hbar^3}|D_{fi}|^2, \tag{8'}$$

where m is the reduced effective mass and $D_{fi}(\mathbf{K})$ is the dipole sum defined in Appendix A. We use the δ function $\delta(E_f-E_i)$ instead of $\Delta(E_f-E_i)$, because the condition $[(\hbar^2/2M)K'^2+(\hbar^2/2m)k'^2+E_2]-[(\hbar^2/2M)K^2+E_1]=0$ can be satisfied. The summation over $\mathbf{k}'$ yields $md^2/\pi\hbar^2$ through application of the relations

$$\frac{1}{N}\sum_{\mathbf{k}}\rightarrow\frac{L^2}{N}\int d^2\mathbf{k}=\frac{mL^2}{N\pi\hbar^2}\int dE_f$$

and $N=(L/d)^2$. After this, the new quantity (8′) is introduced into the thermal average as before. The final result is the same as that which would be obtained by simply replacing $|F(0)|^2\Delta(E_f-E_i)=(8d^2/\pi a_B^2)\Delta(E_2-E_1)$ by $md^2/\pi\hbar^2$ in Eq. (12):

$$w_{fi}^{\text{Stokes}}=\frac{128m(\mu_f\mu_i/\varepsilon)^2}{a_B^2\hbar^3b^2}\,a(b,T). \tag{13}$$

Again, the rate varies essentially as b^{-4}.

C. Numerical results

Aside from the major experimental variables b and T, there are three different types of quantities to consider when applying (12) and (13) to the quantum well data discussed in Sec. II. First and simplest are the fixed parameters a_B, ε, m, and the two-dimensional nearest-neighbor distance d. Next, the transition dipole moments must be chosen, and finally the overlap factor $\Delta(E_2-E_1)$ that appears only in the anti-Stokes rate.

1. Fixed parameters

The dielectric constant appropriate to $1s$ exciton binding is the square of the refractive index, $\varepsilon=n^2$. In our case $n=3.52$,[18] so $\varepsilon=12.39$. Combined with the reduced effective mass of $m=0.046m_e$ (m_e=electron mass), this produces a bulk exciton Bohr radius $a_B=\varepsilon\hbar^2/me^2=14.26$ nm. The electron and hole masses involved are $0.067m_e$ and $0.146m_e$, respectively.[19]

For future reference, the parameter u in the function $a(u)$ depends on M, the total (translational) mass of the exciton. We have $u=b\sqrt{2Mk_BT/\hbar^2}$, and using $M=0.213m_e$,[20] $u=0.021\,96b\ (\text{nm})\sqrt{T\ (\text{K})}$. The nearest-neighbor distance in the square lattice representing one layer of GaAs is $d=a/\sqrt{2}=5.653/\sqrt{2}=4.00$ Å (Ref. 21, p. 848). This produces a two-dimensional envelope function $F(0)=\sqrt{8d^2/\pi a_B^2}=0.0448$.

2. Transition moments

The model we have adopted is based on donor-acceptor energy transfer by electromagnetic interaction of transition dipoles in the near zone. These transition dipole moments play roles in the electronic structure and optical properties of the semiconductors and are, therefore, obtainable experimentally, in principle. One manifestation is the longitudinal-transverse (L-T) splitting of the exciton.[17,20] The transition dipoles are also the same as those participating in ordinary far zone optical transitions and can therefore be extracted, also in principle, from the quantum well absorption and emission spectra.

The L-T splitting is related to the transition dipole moment by[20]

$$\Delta_{\mathrm{LT}}=\frac{4\pi|F^{\mathrm{bulk}}(0)|^2|\mu|^2}{\varepsilon}, \tag{14}$$

where $F^{\mathrm{bulk}}(0)=\sqrt{1/\pi a_B^3}$ is the bulk $1s$ exciton envelope function at the origin. Employing $\Delta_{\mathrm{LT}}=0.08\pm0.02$ meV (Ref. 20) and the fixed parameters, we find

$$|\mu|^2=\frac{\varepsilon\Delta_{\mathrm{LT}}a_B^3}{4}=723\pm180\ \ \mathrm{meV\ nm}^3=(7.0\pm0.9\ \ e\ \text{Å})^2. \tag{15}$$

The dipole matrix element can be related to the absorption coefficient of the individual wells as follows:[17]

$$|F_{\nu'}(0)\mu_f|^2=\frac{n\hbar c}{4\pi^2E_f}\,\pi\gamma_f\sigma_{\max}(E_f). \tag{16}$$

The new symbols in this equation are n, the index of refraction, $\sigma_{\max}(E_f)$, the absorption cross section of the acceptor at the peak, and γ_f, the width [half width at half maximum (HWHM)] of this absorption. The final three factors $\pi\gamma_f\sigma_{\max}(E_f)$ represent the energy-integrated absorption cross section for a line of assumed Lorentzian shape.

Although in our simplified theory the two wells are approximated by two-dimensional (and therefore identical) structures, the transition moments, as determined by experiment, will generally be specific to the well width. The connection between cross section and optical-absorption coefficient $\alpha(E)$ is normally given by $\sigma(E)=n_0^{-1}\alpha(E)$, where n_0 is the number density of absorbers. In the case of the quantum well, one must use $n_0^{-1}=L_zd^2$ for the reasons given in connection with the final states in the transfer probability. That is, the quantum well effect pushes all but one state out of resonance with the absorbed photon. When this value of n_0 and the exciton envelope function $F(0)=\sqrt{8d^2/\pi a_B^2}$ are employed in (16), we have

$$|\mu_f|^2=\frac{L_za_B^2\lambda_fn}{64\pi^2}\int\alpha(E)dE. \tag{17}$$

Here, λ_f is the wavelength corresponding to the peak acceptor absorption and n is the index of refraction. This result corresponds to that of Masumoto *et al.*[15] [see their Eqs. (1) and (3), in which M_{cv} refers to a momentum matrix element]. Using (17), $L_z=5$ nm, and the NW integrated absorption coefficient 700 cm^{-1} eV,[15] we obtain $|\mu_f|=4.7\ \ e$ Å; for $L_z=10$ nm, and the WW integrated absorption coefficient 200 cm^{-1} eV, the result is $|\mu_f|=3.7\ e$ Å. While these transition moments derived from absorption do not quite fall within the range of values predicted by the L-T splitting, Eq. (15), their values are entirely reasonable. We adopt the value $5.5\pm2\ e$ Å with confidence that our final calculation results in the correct order of magnitude.

The analogy of our mechanism with the Förster mechanism also suggests a determination of the transition moments from the radiative emission rate $w_{r,\mathrm{donor}}$:

$$w_{r,\mathrm{donor}}=\frac{4nE_i^3}{\hbar^4c^3}\left[\frac{2\pi\hbar^2}{d^2M}\,\frac{r(T)}{\Delta(T)}\right]|F_\nu(0)\mu_i|^2. \tag{18}$$

The factor in square brackets is a correction due to exciton coherence[22] and is unity for atomic and molecular transitions. The ratio $r(T)/\Delta(T)$ is the fraction of excitons lying within the emission bandwidth when a Boltzmann distribution is established among the excitons, the emission probability of which has been enhanced by the factor $2\pi\hbar^2/d^2M$. For the calculated radiative lifetime of 25 ps for a 100-Å GaAs quantum well,[23] we obtain a transition moment of 3 e Å, corroborating our other estimates.

3. The emission-absorption overlap factor

The factor $\Delta(E_2-E_1)$ in the anti-Stokes expression (12) is, by definition, the overlap of two normalized bands centered at E_1 with width γ_1 and at E_2 with width γ_2 (all HWHM). The excitons in our samples are inhomogeneously broadened. In our calculations we have adopted a homogeneous line shape described by a Lorentzian for the donor and an inhomogeneous line shape described by Gaussian for the acceptor well, based on the argument that there is one initial state, but a sum over final states. We take the donor band to have the Lorentzian form

$$L_d(E)=\frac{\gamma_d}{\pi}\left(\frac{1}{(E-E_d)^2+\gamma_d^2}\right), \tag{19a}$$

and the acceptor band to have the Gaussian form

$$G_a(E)=\frac{1}{\sqrt{2\pi\sigma_a}}\exp\left(-\frac{(E-E_a)^2}{2\sigma_a^2}\right), \tag{19b}$$

where $\sigma_a=\gamma_a/\sqrt{2\ln2}$. With these forms, the overlap is

$$\begin{aligned}\Delta(E_a-E_d,T)&=\int L_d(E)G_a(E)dE\\&=\frac{\gamma_d(T)}{\pi[(E_a-E_a)^2+\gamma_d(T)^2]}\left[1+\frac{\gamma_a(T)^2}{4\ln2}\right.\\&\left.\times\frac{(E_a-E_d)^2-\gamma_d(T)^2}{[(E_a-E_d)^2+\gamma_d(T)^2]^2}+\cdots\right].\end{aligned} \tag{20}$$

This expression is valid when the bands are well separated with respect to their widths. The first term in the square bracket corresponds to replacing the Gaussian with a δ function, and the second is a Taylor-series correction that is of the order of 10^{-6}. The temperature dependence and its source are emphasized here. The WW-NW peak energy difference is 60 meV (Fig. 1). The half width of the emission band (γ_1, for the donor well) is taken as $0.055+0.00125T$ in

meV, where T is the temperature,[24] and that of the absorption band (γ_2, for the acceptor well) is similarly $0.225+0.0025T$.[25]

The overlap factor is essentially a linear function of temperature because of the dominance of the peak difference in its denominator. Its value (at $T=4$, 20, 40, 60, 80, 100 K) is $(0.531, 0.707, 0.928, 1.15, 1.37, 1.59)\times 10^{-5}$ (meV^{-1}).

4. Summary

The numerical values of the anti-Stokes and Stokes transfer rates evaluated at $b=17.5$ nm and $T=4$ K are

$$w_{fi}^{\text{anti-Stokes}}=\frac{4\pi}{\hbar}\left(\frac{16\mu_f\mu_i}{a_B^2\varepsilon}\right)^2\frac{1}{b^2}a(b,T)\Delta(E_f-E_i,T)$$

$$=(1.46\times 10^{14}\ \text{meV nm}^2\ \text{s}^{-1})\frac{1}{(17.5\ \text{nm})^2}$$

$$\times a(17.5\ \text{nm},\ 4\ \text{K})\Delta(60\ \text{meV},\ 4\ \text{K})$$

$$=1.20\times 10^6\ \text{s}^{-1},$$

$$w_{fi}^{\text{Stokes}}=\frac{128m}{\hbar^3}\left(\frac{\mu_f\mu_i}{a_B\varepsilon}\right)^2\frac{1}{b^2}\,a(b,T)$$

$$=(7.15\times 10^{11}\ \text{nm}^2\ \text{s}^{-1})\frac{1}{(17.5\ \text{nm})^2}$$

$$\times a(17.5\ \text{nm},\ 4\ \text{K})$$

$$=1.10\times 10^9\ \text{s}^{-1}.$$

The full dependence on well spacing and temperature, deriving from b^{-2},$a(b,T)$, and the overlap factor, are shown in Figs. 5(a),5(b).

IV. DISCUSSION

A. Comparison with experiments

Several comments can be made on comparison between the experimental results and the numerical calculations based on the Förster-Dexter theory of energy transfer applied to quantum wells. First, the calculation reproduces the order-of-magnitude of the transfer rate. The calculation also reproduces the weak temperature dependence of the experiments, although it appears that the experiment and the theory show opposite trends. The most glaring discrepancy is that the experiments, rather surprisingly, show a reduced transfer rate for thinner barriers, whereas the theory predicts increased transfer rates for thinner barriers, as one might expect from intuitive arguments. Although finite well thickness and line shapes may affect the theoretical results, it is more likely that variation of the linewidths of different samples is the primary cause of this discrepancy. We examine some of the approximations in the theory in B, and some alternate models in C.

B. Approximations

The application of resonance transfer theory to the quantum well problem carriers with it many approximations, some of which are not easily controlled. We summarize the important ones here without detailed assessment, which would require a view based on a more comprehensive theory that does not presently exist.

(i) First-order time-dependent perturbation theory is applied, using a multipole expansion that is cut off at the dipole-dipole term. In the case of intermolecular transfer, this approximation breaks down when the molecular size is comparable with the intermolecular distance. A satisfactory theory is available through the ''monopole approximation.''[26] The validity of our cutoff is reasonable despite the large dimensions of the donor and acceptor because, by using Wannier excitons, the monopole approximation is essentially being used.

(ii) The transition dipole moments used are indirectly evaluated, taken from experiments on optical properties of related materials. This is discussed in Sec. II B, where a probable error of $\pm 40\%$ was estimated.

(iii) The Förster method is used to estimate the density of final states for anti-Stokes transfer. This approximation is consistent with the use throughout of optical properties for the indirect evaluation of parameters, and corresponds physically to assuming a multiphonon transfer mechanism. Note also that in the spirit of the Förster method, we have assumed a metastable thermal equilibrium distribution of the initial states before transfer. We have not considered the question of how such a distribution is achieved following excitation by a cw laser.

(iv) The widths of the quantum wells are assumed negligible, i.e., a two-dimensional model of the exciton is adopted, and the separation parameter is taken as the well-center–to–well-center distance. The excitons involved are associated with the lowest quantum well states and, therefore, have their largest z-direction amplitude at the center of the wells. The effect of the reduction of the oscillator strength, due to the quantum well effect, is discussed in Sec. III A. We have estimated the effect of the z dependence of the wave function on the transfer rate, and find that a possible factor of $\frac{9}{16}$ is omitted by neglecting it. However, any inhomogeneities in the wells will tend to reduce the quantum effect on the density of states, which makes an unknown correction in the opposite direction. This correction could be of the same order of magnitude, so we can assign a probable error of $\pm 50\%$ to these sources.

(v) The absorption and emission bands are approximated by Lorentzian or Gaussian line shapes. The use of a homogeneously broadened (Lorentzian) line shape for the exciton in the donor well is very reasonable and should introduce errors much smaller than those mentioned above. The use of Gaussian line shape for the exciton in the acceptor well, and the role of Urbach tail in determining the line shape need further investigation, and the present calculation using Gaussian acceptor line shape should be considered as a lower limit. In summary, the quantifiable sources of error produce an uncertainty of about a factor of two in the predicted results.

C. Alternative models

We examine here other possible models to explain the experimental results. The model should provide WW exciton luminescence by NW excitation and *vice versa*, and it should also explain the lack of dependence on temperature and bar-

rier thickness. The models to be considered are as follows: thermal activation, tunneling, defect-related direct transition, two-photon absorption (TPA) in the NW, and dipole-dipole transfer.

In the thermal activation model, carriers escape from a well and diffuse to the other well with a diffusion constant D. Therefore, this model will yield a linear dependence of energy transfer rate on barrier thickness, $\tau_1 = bD^{-1/2}$. This dependence may not contradict the experiment, if we assume a sample-dependent nonradiative lifetime. The temperature dependence, however, disagrees with the experiment. Thermal activation should provide a strong dependence like $\exp[-(E_B - E_i)/kT]$, where E_B is the barrier height and E_i is a quantum level. Moreover, this energy transfer is ineffective at low temperatures; the thermal activation probability is 5×10^{-7}, even at 80 K for $E_B - E_i = 100$ meV.

Probability of tunneling of carriers will show a weak temperature dependence. However, it will be an exponential function of barrier thickness. Thick barriers yield tunneling times which are too long ($\sim$300 ns for a 30-nm-thick barrier, even if the electron sublevel in the NW is resonant to the second electron sublevel in the WW) to explain the experiment. A model of a leaky barrier resulting from the alloy nature of the barrier was recently presented by Kim *et al.*[27] The basic idea is that the random nature of the alloy contributes to high transfer efficiency in samples with $Al_xGa_{1-x}As$ barriers with small x. This appears to be a promising alternative model that needs to be further considered. Note, however, that this model predicts no transfer for binary barriers. Transfer between $In_xGa_{1-x}As$ quantum wells separated by binary InP barriers has been reported previously by Sauer, Harris, and Tsang.[28] We have applied our theory to the results of Sauer, Harris, and Tsang and although the peaks are not resolved, an order of magnitude agreement is found between our theory and the experiments.

If the NW contains a defect level that coincides with the exciton level in the WW, one may observe a NW exciton luminescence enhancement by a two-step excitation involving the defect level when the excitation is at the WW exciton energy. However, low absorption at defects makes this unlikely. Also, it is unlikely that all three different samples (sample *A* was grown at a different time and by a different growth chamber than the one that was used for samples *B* and *C*) happen to have a defect level at the exciton level of the wide well.

The NW exciton can be excited by a lower-energy photon by two-photon absorption, which may be resonantly enhanced by the WW exciton. This process should be examined quantitatively, and is open for further study. However, we observe that the transfer efficiency is independent of the excitation intensity over the range of about a factor of 10 investigated in our experiments. Recently, Hellman *et al.*[29] have reported anti-Stokes energy transfers to barriers in *II-VI* quantum wells of $Cd_xMn_{1-x}Te$ with relatively large total barrier thickness (of the order of 1 μm). These authors find that reabsorption of photons emitted by the quantum wells by two-step absorption involving defect states in the barrier is responsible for anti-Stokes luminescence of the barrier observed in their case. The measured intensity dependence, the resonant nature of our anti-Stokes transfer and relatively thin barriers makes two-photon absorption involving defect states an unlikely explanation in our case.

So far, we see that only dipole-dipole energy transfer reproduces the experimental results on the magnitude and temperature dependence of the transfer efficiency. Dipole-dipole interaction must therefore be considered as a likely mechanism for the efficient transfer observed between widely separated quantum wells at low temperatures. It is interesting to note that our theory may also be applicable to a different system. Recently, Lawrence *et al.*[30] have observed ''exciton tunneling'' between $CdTe/Cd_xMn_{1-x}Te$ and $CdTe/Cd_xZn_{1-x}Te$ quantum wells, using geometries similar to ours. Their observed transfer rates (3.3×10^{10} s^{-1} and 3.6×10^{9} s^{-1} in two different $CdTe/Cd_xMn_{1-x}Te$ samples, and about 5×10^{10} s^{-1} for the $CdTe/Cd_xZn_{1-x}Te$ sample) are of the same order of magnitude as those we have found, but the high rates were apparently possible only under resonant conditions, or explicit involvement of LO phonons. Thus, the intrinsic electronic matrix elements may have been much smaller than ours, indicating a process of the Dexter exchange type.[6] There the Forster dipole-dipole matrix elements are essentially replaced by products of electron-electron and hole-hole overlaps between the wells. Such an interpretation, based on our formalism, provides a microscopic interpretation of the term ''exciton tunneling,'' or correlated electron-hole tunneling. Its rate should exhibit a rapid drop upon increase in barrier thickness, just as in the case of ordinary carrier tunneling.

V. CONCLUSIONS

We have observed efficient energy transfer at low temperatures between excitons in two unequal quantum wells separated by wide and high barriers. We have also observed a weak anti-Stokes energy transfer from the wide-well exciton to the narrow well exciton under similar experimental conditions. The transfer efficiency is almost independent of temperature and barrier thickness, which cannot be explained by tunneling and thermal activation over the barriers. We have investigated dipole-dipole interaction as a transfer mechanism, which has not been previously considered for energy transfer between quantum wells. The dipole-dipole energy-transfer model provides the correct temperature dependence and magnitude for the transfer efficiency, but does not explain the independence on barrier thickness. Further experimental and theoretical studies should be valuable in understanding these interesting observations.

ACKNOWLEDGMENTS

The authors thank D. S. Kim, S. W. Koch, and P. Thomas for many valuable discussions, J. M. Kuo for providing some of the samples for this study, and T. C. Damen and D. S. Kim for their contributions in the early stages of this research. The research of one of the authors (R.S.K.) was supported in part by the Sponsors of the Laser Fusion Feasibility Project of the Laboratory for Laser Energetics (University of Rochester).

APPENDIX A: CALCULATION OF THE SQUARE OF THE INTERACTION MATRIX ELEMENT

The derivation of text Eq. (6) will be sketched here. We first consider the lattice sum. The vector $\mathbf{R}$ is the position of the transferred Wannier exciton in the acceptor well relative to its original position at the origin of the donor well. Therefore, $\mathbf{R}=R_x\hat{\mathbf{x}}+R_y\hat{\mathbf{y}}+b\hat{\mathbf{z}}$ where b is the well separation. The wells are assumed two dimensional in the xy plane, parallel to one another. The transition moment $\boldsymbol{\mu}_i$ is taken to be $\mu_i\hat{\mathbf{x}}$ and that of the final state is $\boldsymbol{\mu}_f=\mu_f(\cos\phi_0\hat{\mathbf{x}}+\sin\phi_0\hat{\mathbf{y}})$. In both cases, the moment is that of a transition between Wannier functions located on the same cell, because the envelope function has already been factored out [Eqs. (4), (6)]. We thus obtain

$$D_{fi}(\mathbf{K})=\sum_{\mathbf{R}} e^{i\mathbf{K}\cdot\mathbf{R}}\frac{\mu_f\mu_i}{\varepsilon R^5}[(R^2-3R_x^2)\cos\phi_0-3R_xR_y\sin\phi_0], \tag{A1}$$

with $R=(R_x^2+R_y^2+b^2)^{1/2}=(r^2+b^2)^{1/2}$, where $r=(R_x^2+R_y^2)^{1/2}$. We now transform to polar coordinates in $\mathbf{K}$ and $\mathbf{R}$, such that $K_x=K\cos\phi_K$, $K_y=K\sin\phi_K$, $R_x=r\cos\phi$, and $R_y=r\sin\phi$. The lattice sum is converted to an integral by the approximation

$$\sum_{\mathbf{R}} \rightarrow \lim_{N,R\rightarrow\infty}\frac{N}{\pi R^2}\int_0^R r\,dr\int_0^{2\pi}d\phi$$

$$\rightarrow n_a\int_0^{\infty} r\,dr\int_0^{2\pi}d\phi,$$

in which a large circular finite lattice of N points with n_a lattice points per unit area is effectively made into a continuum. With the further definition $\alpha=\phi-\phi_K$, the lattice sum becomes

$$D_{fi}(\mathbf{K})=n_a\int_0^{\infty} r\,dr\int_0^{2\pi}d\alpha\; e^{iKr\cos\alpha}\frac{\mu_f\mu_i}{\varepsilon(r^2+b^2)^{3/2}}[\cos\phi_0$$

$$-3\left(\frac{r^2}{r^2+b^2}\right)g(\phi_K,\phi_0,\alpha)],$$

where

$$g(\phi_K,\phi_0,\alpha)\equiv(\cos^2\phi_K\cos^2\alpha+\sin^2\phi_K\sin^2\alpha)\cos\phi_0$$

$$+\cos\phi_K\sin\phi_K\cos2\alpha\;\sin\phi_0.$$

The α integrals can be expressed as Bessel functions, $J_0(Kr)$ and $J_1(Kr)$, after which the radial integrals may be evaluated as elementary functions. The result is

$$D_{fi}(\mathbf{K})=\frac{2\pi n_a\mu_f\mu_i}{\varepsilon b}\cos\phi_0[1+\cos^2\phi_K+(Kb-3)\sin^2\phi_K$$

$$+\sin\phi_0(4-Kb)\cos\phi_K\sin\phi_K].$$

We now sum the square of the matrix element over rings of constant energy by averaging over ϕ_K with the result

TABLE I. The function $a(u)$ at various values of T (K) and b (nm). See text, Eqs. (9) and (10).

T (K)	$b=17.5$ nm	$b=27.5$ nm	$b=37.5$ nm
4	0.472 42	0.295 86	0.186 89
10	0.293 51	0.144 86	0.084 89
20	0.173 98	0.080 19	0.048 90
30	0.121 87	0.059 15	0.031 83
40	0.094 98	0.045 24	0.024 09
50	0.079 43	0.035 39	0.019 40
60	0.069 31	0.029 66	0.016 26
70	0.061 80	0.025 54	0.014 01
80	0.055 55	0.022 45	0.012 31
90	0.049 89	0.020 03	0.010 98
100	0.044 61	0.018 08	0.009 92

$$|D_{fi}(K)|^2=\frac{4\pi^2n_a^2\mu_f^2\mu_i^2}{\varepsilon^2b^2}[2-Kb+K^2b^2(\tfrac{3}{8}\cos^2\phi_0$$

$$+\tfrac{1}{8}\sin^2\phi_0)]. \tag{A2}$$

We reserve the bracket notation $\langle\,\rangle$ for the thermal average (Appendix B).

The angle ϕ_0 has been arbitrary up to this point. It represents the direction of the transition moment in the acceptor well, with respect to that of the moment of the initial state in the donor well. Because the acceptor well has two orthogonal degenerate states that can participate in the transfer, we sum (A2) over two terms, one with an arbitrary value of ϕ_0 and the other with the value $\phi_0+\pi/2$. The result is independent of ϕ_0 and produces the terms that result in the second line of Eq. (6) of the text.

The exciton envelope functions are those of the lowest ''1s'' states[31] and are taken to be the same for each well in the two-dimensional approximation. Thus, in each case $F(0)=\sqrt{8d^2/\pi a_B^2}$, where d is the nearest-neighbor distance and a_B is the Bohr radius of the bulk exciton, $a_B=\varepsilon\hbar^2/me^2$. Taking $n_a=d^{-2}$, which accounts for the fact that only one two-dimensional exciton is in resonance because of the z-direction quantum effect, we obtain $|F(0)|^4(4\pi^2n_a^2)=(16/a_B^2)^2$ and hence the third line of Eq. (6).

APPENDIX B: NOTES ON THE FUNCTION $a(u)$

The conversion of the thermal average, Eq. (9), into the function $a(u)$, Eq. (10), is a straightforward but tedious process. However, finding the dependence of $a(u)$ on u in practical terms is not at all straightforward. The values of u required are neither very small nor very large, ranging from 0.768 at 17.5 nm and 4 K to 8.23 at 37.5 nm and 100 K.

The asymptotic expansion of $\sqrt{\pi}u\,\exp(u^2)\mathrm{erfc}(u)$ is a power series in u^{-2} [see, e.g., Abramowitz and Stegun (Ref. 32, p. 298)]. When this expansion is substituted in (10), the apparent character of the function changes entirely, to the form (11), because of the complete cancellation of the terms u^4, $5u^2$, and 8. The remaining terms do not converge rapidly over much of the required range and extremely high accuracy is required in the function $\exp(u^2)\mathrm{erfc}(u)$.

Table I shows the results of a combination of methods for

determining $a(u)$. Generally, the best method was the use of interpolations of the erfc(u) values for large u, found in Ref. 32, p. 316. This was least useful for $u<3.75$, which is the case for all the $T=4$ K values and the 10- and 20-K values for $b=17.5$ nm. Here, a numerical method from MATLAB® was employed for erfc(u). The fitted expression shown in the text is based on the form $\ln[a(u)]=-0.529\,75-1.9371[\ln(u)]$, with $R^2=1.000$ over the range $u=3.75-14$.

*On leave from NEC Corporation, Japan. Present address: Opto-Electronics Research Laboratories, NEC Corporation, 34 Miyukigaoka, Tsukuba, Ibaraki 305, Japan.

†Also at Department of Physics and Astronomy, University of Rochester, Rochester, NY 14627-0171.

[1] L. Esaki and R. Tsu, IBM J. Res. Dev. **14**, 61 (1970).

[2] J. Shah, K. Leo, D. Y. Oberli, and T. C. Damen, in *Ultrashort Processes in Condensed Matter*, edited by W. E. Bron (Plenum, New York, 1993), p. 53.

[3] H. X. Jiang, E. X. Ping, P. Zhou, and J. Y. Lin, Phys. Rev. B **41**, 12 949 (1990).

[4] A preliminary report of the experimental results was presented by A. Tomita, J. Shah, D. S. Kim, T. C. Damen, J. M. Kuo, S. Schmitt-Rink, P. Thomas, and R. S. Knox, at *QELS'92* and *IQEC'92*, International Quantum Electronics Conference Technical Digest Series 9 (IEEE, Piscataway, NJ, 1992), p. 102.

[5] Th. Förster, Ann. Phys. (Leipzig) **2**, 55 (1948).

[6] D. L. Dexter, J. Chem. Phys. **21**, 836 (1953).

[7] R. Flach, D. S. Hamilton, P. M. Selzer, and W. M. Yen, Phys. Rev. Lett. **35**, 1034 (1975).

[8] T. Holstein, S. K. Lyo, and R. Orbach, Phys. Rev. Lett. **36**, 891 (1976).

[9] M. Stavola, D. L. Dexter, and R. S. Knox, Phys. Rev. B **31**, 2277 (1985).

[10] T. Takagahara, Phys. Rev. B **31**, 6552 (1985).

[11] B. S. Wang and J. L. Birman, Phys. Rev. B **43**, 12 458 (1991).

[12] T. Hiroshima, E. Hanamura, and M. Yamanishi, Phys. Rev. B **38**, 1241 (1988).

[13] C. C. Sung and G. Mo, Phys. Rev. B **38**, 3618 (1988).

[14] M. Batsch, T. Meier, P. Thomas, M. Lindberg, S. W. Koch, and J. Shah, Phys. Rev. B **48**, 11 817 (1993).

[15] Y. Masumoto, M. Matsuura, S. Tarucha, and H. Okamoto, Phys. Rev. B **32**, 4275 (1985).

[16] These lifetimes were measured with nonresonant excitation, and correspond to the lifetime of thermalized excitons. This is the appropriate lifetime to use in the transfer rate calculation, since a large majority of excitons are thermalized in a cw experiment.

[17] R. S. Knox, *Solid State Physics: Advances in Research and Applications*, edited by F. Seitz and D. Turnbull (Academic, New York, 1963), Suppl. 5, p. 37.

[18] J. S. Blakemore, J. Appl. Phys. **53**, R123 (1982).

[19] The average hole mass, defined as $2/m_h=1/m_{\rm hh}+1/m_{\rm lh}=\gamma_l$, and the electron mass are obtained from *Physics of Group IV Elements and III-V Compounds*, edited by O. Madelung, Landolt-Börnstein, New Series, Group III, Vol. 17, Pt. a (Springer-Verlag, Berlin, 1982), pp. 222–223.

[20] R. G. Ulbrich and C. Weisbuch, Phys. Rev. Lett. **38**, 865 (1977).

[21] S. M. Sze, *Physics of Semiconductor Devices*, 2nd ed. (Wiley, New York, 1982).

[22] J. Feldman, G. Peter, E. O. Göbel, P. Dawson, K. Moore, C. Foxon, and R. J. Elliott, Phys. Rev. Lett. **59**, 2337 (1987).

[23] L. C. Andreani, F. Tassone, and F. Bassani, Solid State Commun. **77**, 641 (1991). A radiative lifetime of 40 ps was determined for a 150-Å GaAs quantum well from time-resolved luminescence studies by A. Vinattieri, J. Shah, T. C. Damen, D. S. Kim, L. N. Pfeiffer, M. Z. Maialle, and L. J. Sham, Phys. Rev. B **50**, 10 868 (1994).

[24] A. Honold, L. Schultheis, J. Kuhl, and C. W. Tu, *Ultrafast Phenomena VI*, edited by T. Yajima, K. Yoshihara, C. B. Harris, and S. Shionoya (Springer-Verlag, Berlin, 1988), p. 307. See, also, A. Honold *et al.* Phys. Rev. B **40**, 6442 (1989).

[25] L. Schultheis, A. Honold, J. Kuhl, K. Köhler, and C.W. Tu, Phys. Rev. B **4**, 9027 (1986).

[26] F. London, J. Phys. Chem. **46**, 305 (1942).

[27] D. S. Kim, H. S. Koh, Y. M. Kim, S. J. Rhee, W. S. Kim, and J. C. Woo, Bull. Am. Phys. Soc. **40**, 76 (1995).

[28] R. Sauer, T. D. Harris, and W. T. Tsang, Appl. Phys. Lett. **50**, 1077 (1987).

[29] R. Hellman, A. Euteneuer, S. G. Hense, J. Feldmann, P. Thomas, E. O. Göbel, D. R. Yakovlev, A. Waag, and G. Landwehr, Phys. Rev. B **51**, 18 053 (1995).

[30] I. Lawrence, S. Haacke, H. Mariette, W. W. Rühle, H. Ulmer-Tuffigo, J. Cibert, and G. Feuillet, Phys. Rev. Lett. **73**, 2131 (1994).

[31] S. Schmitt-Rink, D. S. Chemla, and D. A. B. Miller, Adv. Phys. **38**, 89 (1989).

[32] M. Abramowitz and I. A. Stegun, *Handbook of Mathematical Functions* (National Bureau of Standards, Dover, 1965).